Journal of Vibration Engineering & Technologies (2023) 11:3147–3162
https://doi.org/10.1007/s42417-022-00737-z

ORIGINAL PAPER

Reliability-Based Optimization of Flexible Manipulators

Fabian Andres Lara-Molina[1] · **Rogério Sales Gonçalves**[2]

Received: 17 May 2022 / Revised: 26 August 2022 / Accepted: 4 October 2022 / Published online: 20 October 2022

Abstract

Purpose This paper addresses the optimal design of flexible link manipulators to optimize the dynamic performance subject to the effect of the uncertainties quantified by a reliability index.

Methods The links' uncertain stiffness and inertial parameters are modeled using the stochastic finite-element method. A methodology is proposed to determine the design variables that maximize the performance and simultaneously maximize reliability that aims to optimize the flexible manipulators based on reliability-based optimization. This reliability-based optimization derives a multi-objective optimization problem that is solved using evolutionary algorithms.

Results Numerical results illustrate the dynamic modeling of the one-link flexible manipulator using the stochastic finite element method in terms of displacement of the manipulator's tip and the frequency response function subjected to uncertainties. Moreover, the optimal design was carried out to maximize the reliability and optimize the elastodynamic performance; thus, the reliability of the manipulator is maximized, and several performance criteria such as the actuator power, manipulator mass, and the first mode natural frequency are optimized simultaneously.

Conclusions The proposed methodology permitted optimizing critical operational characteristics of flexible manipulators, such as minimizing the elastic deflections, minimizing the power of actuators, and minimizing the mass of the manipulator subject to reliability constraints. Thus, the main contributions are (i) the stochastic modeling of flexible-link manipulators, (ii) the reliability optimization approach applied to the flexible-link manipulator, and (iii) a case study considering a one-link flexible manipulator with uncertain structural parameters to determine the optimal inertial parameters and geometric parameters.

Keywords Reliability · Flexible-link manipulator · Optimization · Uncertainty

Introduction

The application of robotic manipulators demands increasing the operational speed and simultaneously decreasing the weight in several areas such as automation manufacturing, hazardous tasks, and medical applications [1]. These operational requirements result in lightweight manipulators with thin links subject to residual vibrations during the task executions that reduce dynamic performance. On the other hand, the unavoidable effect of uncertainties also reduces performance. Moreover, robots are designed for close human–robot cooperation; these manipulators with slender links have compliant links and joints that reduce the impact in a potential collision [2]; Nevertheless, they exhibit undesired vibration [3]. There is a vast literature about the control of robots with flexible elements and uncertainties [4, 5]; Nevertheless, few contributions have addressed the optimal design. The optimal design has been applied to enhance the dynamic performance of manipulators with flexible elements [6, 7]. These research works have emphasized the need to propose novel methodologies to optimize the design of flexible manipulators by including the harmful effects of uncertain parameters.

The robust optimal design optimizes the system performance and simultaneously minimizes the adverse consequences of uncertainties simultaneously [8]. Several works have focused on the robust optimal design of manipulators

✉ Fabian Andres Lara-Molina
fabian.molina@uftm.edu.br

Rogério Sales Gonçalves
rsgoncalves@ufu.br

[1] Department of Mechanical Engineering, Federal University of Triângulo Mineiro, Uberaba, MG, Brazil

[2] School of Mechanical Engineering, Federal University of Uberlândia, Uberlândia, MG, Brazil

to optimize the kinematic and dynamic performance subject to dimensional tolerances of geometric parameters, joint clearances, noise sensors, and variability of inertia parameters. The optimal design of parallel robots was carried out based on the robust criteria and elastodynamics [9]. The robust multi-objective optimal design to optimize the performance of parallel manipulators subject to uncertainties was also proposed; this robust optimization consists of a multi-objective optimization problem that aims at optimizing the performance and robustness criterion simultaneously [10]. These research studies aim at optimizing the performance subject to the unavoidable effect of uncertainties. The reliability-based optimization has been proposed as an alternative approach to robust design optimization [11]. Thereby, the effect of the uncertainty is quantified by a measure of reliability. The robotic system's dynamic performance was optimized for high reliability under uncertainty [12].

Several numerical methods have been developed to enhance computational cost and accuracy of robust optimal design applied to optimize mechanical structures subject to uncertain operational conditions. A Hierarchical Model Updating Strategy was implemented for Finite Element model updating to establish an accurate computational model [13]. A synchronous modeling concept is proposed, the purpose of which is to realize the transformation from single-objective reliability design to multiple objectives reliability design [14]. In the same direction, multilevel nested models were developed to effectively perform the reliability-based design optimization of the assembly relationship [15]. These developments in reliability computation and reliability-based design optimization permitted to carry out of further engineering applications. Li et al. [16] developed a method to identify the modal parameters of damped oscillation signal in a power system; this application demonstrated the potential benefits of the numerical methods to improve the efficiency of reliability computation. Moreover, Fei et al. [17] evaluated the motion reliability of flexible mechanism; they demonstrated that the enhancement of the network learning model with an intelligent operator ameliorated the reliability computation in terms of simulation efficiency to design procedures.

Several studies have been developed to evaluate the reliability of the flexible mechanisms. In [18], the kinematic reliability of robotic manipulators based on the fuzzy theory was proposed without considering the link flexibility. To improve the computational efficiency of the reliability-based design optimization of flexible manipulators in [19], particle swarm optimization together with an advanced extremum response surface method was used with better results. In [20], a genetic algorithm is developed as a reliability model to evaluate the flexible mechanisms under operation. The mean-probability decomposition-coordination-based extreme support vector machine regression method was used in [21] to increase the computational efficiency and accuracy in the reliability optimization of flexible mechanisms.

However, few research studies have been reported about the optimal design of manipulators with flexible elements. The shape optimization of flexible-link manipulators of circular cross-sections was studied, and the method was permitted to obtain the geometry of the manipulator to optimize the dynamic behavior. Shape optimization [6]. The optimal design procedure of a symmetrical 2-DOF parallel planar robot with flexible joints by considering several performance criteria based on the workspace size, dynamic dexterity, and control energy was presented in [7]. The design of a piezo-actuated flexural manipulator was carried out to determine the geometric parameters and maximize the sensitivity [22]. The structural and control optimization of manipulators have been optimized considering the elastic deformation of the manipulator elements [23]. Several works are aimed at optimizing the trajectory planning of flexible manipulators [24, 25]. Nevertheless, no research studies have studied the optimal design of flexible manipulators considering the unavoidable effect of the uncertainties in their physical parameters.

Consequently, a design procedure of flexible manipulators based on reliability-based optimization is introduced in the present contribution to determine the design variables that maximize the elastodynamic performance and reliability by solving a multi-objective optimization problem using multi-objective genetic algorithms. Several methods proposed in the literature have been concerned with the accuracy, and computational cost of reliability-based optimization [13–15]. Nonetheless, the method proposed in this research study is inspired by the work of [26] that solved the reliability optimization problem as a multi-objective optimization problem using evolutionary algorithms. The manuscript presents the following contributions: (i) the stochastic modeling of flexible-link manipulators based on the stochastic finite-element method, (ii) the reliability optimization approach applied to the flexible-link manipulator, (iii) a case study to illustrate the proposed approach applied to a one-link flexible manipulator with uncertain structural parameters to determine the inertial parameters and cross-section dimensions of the link.

The paper is structured as follows: Sect. 2 provides the modeling of flexible-link manipulators with uncertainties by using the stochastic finite-element method. Next, Sect. 3 presents the reliability-based optimization applied to the flexible-link manipulator. Section 4 presents the numerical results. Finally, key conclusions and recommendations are drawn in Sect. 5.

Modeling of Flexible-Link Manipulators with Uncertainties

This paper studies a single-link flexible manipulator with uncertain proprieties within the links. The modeling of the flexible-link manipulator with uncertainties (of Sect. 2.2) was developed as an extension of the modeling of the flexible manipulator based on the Lagrange principle and finite-element model of Sect. 2.1.

The one-link flexible manipulator is presented in Fig. 1a. The manipulator has one revolute joint (ϕ_1), the inertia of the hub is defined as I_{m1}, and a flexible link with length l_1. Moreover, the mass (m_{p1}) is concentrated at the tip of the link.

Modeling of Flexible-Link Manipulator Based on Finite Element Method

The modeling of the one flexible-link manipulator was presented by Usoro et al. [27]. This section presents the main points and results of the modeling using the Lagrange principle and the finite-element method.

The one-link flexible manipulator with length l_1 and n_{1j} elements is presented in Fig. 1a. Initially, the Cartesian position $\mathbf{r}_{1j}$ of each element $1j$ of the link with reference to the inertial reference O is defined as:

$$\begin{aligned}\mathbf{r}_{1j} =& \mathbf{R}(\phi_1, z_1)\mathbf{r}_j \\ =& \begin{bmatrix}\cos(\phi_1) & -\sin(\phi_1)\\ \sin(\phi_1) & \cos(\phi_1)\end{bmatrix} \quad \begin{bmatrix}(j-1)l_{1j} + x_{1j}\\ y_{1j}\end{bmatrix}\end{aligned} \tag{1}$$

with $\mathbf{R}(\phi_1, z_1)$ being the rotation matrix of the joint angle ϕ_1 around the z_1 axis of O_1; $l_{1j} = l_1/n_{1j}$ is the element length; $\mathbf{r}_j$ is the Cartesian position of the element $1j$ with reference to the frame O_1; $\mathbf{r}_j$ is defined for $0 \le x_{1j} \le l_{1j}$ and $j = 1, 2, \ldots, n_{1j}$. It is worth mentioning that y_{1j} corresponds to the transversal displacement that is defined by the shape functions $\Phi(x_{1j})_k$ for $k = 1, \ldots, 4$ [28] according to the following definition:

$$y_{1j}(x,t) = \sum_{k=1}^{4} \Phi_k(x_{1j}) u_{i,2(j-1)+k} \tag{2}$$

Moreover, the generalized coordinates of the element $1j$ are defined as $\mathbf{q}_{1j} = [\phi_1 \ \boldsymbol{\psi}_{1j}]$ with $\boldsymbol{\psi}_{1j} = [u_{1,2(j-1)+1} \ u_{1,2(j-1)+2} \ u_{1,2(j-1)+3} \ u_{1,2(j-1)+4}]$ (see Fig. 1b).

The kinematic energy considers the link elements (T_{1j}), the tip mass ($T_{m_{p1}}$), and the hub inertia ($T_{I_{m1}}$). In addition, the potential energy considers the transversal elastic deformation of the link elements (V_{1j}). The definition of the kinematic and potential energies is presented in Eq. (3).

$$\begin{cases} T_{1j} &= \frac{1}{2}\int_0^{l_{1j}} \rho A \left[\frac{\partial \mathbf{r}_{1j}^T}{\partial t}\frac{\partial \mathbf{r}_{1j}}{\partial t}\right] \mathrm{d}x_{1j} = \frac{1}{2}\dot{\mathbf{q}}_{1j}^T \mathbf{M}_{1j}\dot{\mathbf{q}}_{1j} \\ T_{m_{p1}} &= \frac{1}{2} m_{p1}\left[\dot{\mathbf{r}}_{1j}\mid_{j=n_{1j}, x_{1j}=l_{1j}}\right]^T\left[\dot{\mathbf{r}}_{1j}\mid_{j=n_{1j}, x_{1j}=l_{1j}}\right] = \frac{1}{2}\dot{\mathbf{q}}_{1j}^T \mathbf{M}_{m_{p1}}\dot{\mathbf{q}}_{1j} \\ T_{I_{m1}} &= \frac{1}{2} I_{m1}\dot{\phi}_1^2 \\ V_{1j} &= \frac{1}{2}\int_0^{l_{1j}} EI\left[\frac{\partial^2 y_{1j}}{\partial x_{1j}^2}\right]^T\left[\frac{\partial^2 y_{1j}}{\partial x_{1j}^2}\right] \mathrm{d}x_{1j} = \frac{1}{2}\mathbf{q}_{1j}^T \mathbf{K}_{1j}\mathbf{q}_{1j} \end{cases} \tag{3}$$

where ρ is the mass density, E is Young's modulus, A and I are the area and cross-section moment of the inertia of the link.

The energy of the hub inertia $T_{I_{m1}}$ affects only the elements related to the joint ϕ_1. The elementary mass matrices $\mathbf{M}_{1j}$, $\mathbf{M}_{m_{p1}}$ and the stiffness matrix $\mathbf{K}_{1j}$ are obtained by solving the expressions of Eq. (3):

$$\begin{aligned}\mathbf{M}_{1j} =& \int_0^{l_{1j}} \rho A \left[\frac{\partial \mathbf{r}_{1j}^T}{\partial \mathbf{q}_{1j}}\frac{\partial \mathbf{r}_{1j}}{\partial \mathbf{q}_{1j}}\right] \mathrm{d}x_{1j} \\ =& \frac{\rho A l_{1j}}{420}\begin{bmatrix} m_{11} & m_{12} & m_{13} & m_{14} & m_{15} \\ m_{12} & & & & \\ m_{13} & & \mathbf{M}_{ij}^{\boldsymbol{\psi}_{1j}\boldsymbol{\psi}_{1j}} & & \\ m_{14} & & & & \\ m_{15} & & & & \end{bmatrix}\end{aligned} \tag{4}$$

with $m_{11} = 120(3j^2 - 3j + 1) + \boldsymbol{\psi}_{1j}^T \mathbf{M}_{ij}^{\boldsymbol{\psi}_{1j}\boldsymbol{\psi}_{1j}} \boldsymbol{\psi}_{1j}$, with $\boldsymbol{\psi}_{1j} = [u_{1,2(j-1)+1} \ u_{1,2(j-1)+2} \ u_{1,2(j-1)+3} \ u_{1,2(j-1)+4}]$, $m_{12} = 21(10j - 7)$, $m_{13} = 7l_{1j}(5j - 3)$, $m_{14} = 21(10j - 3)$, $m_{15} = -7l_{1j}(5j - 2)$. $\mathbf{M}_{ij}^{\boldsymbol{\psi}_{1j}\boldsymbol{\psi}_{1j}}$ is defined in the following form:

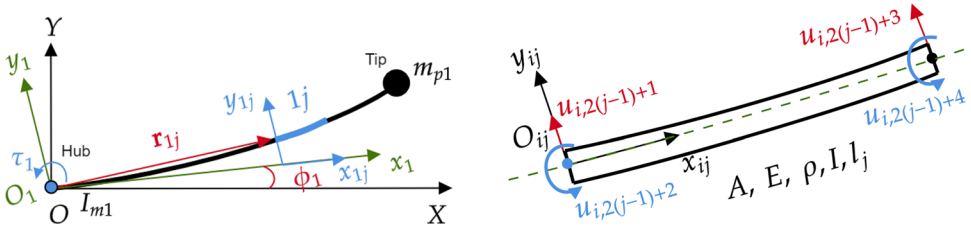

(a) One-link flexible manipulator. **(b)** Link finite-element.

Fig. 1 Model of the one-link flexible manipulator

$$\mathbf{M}_{ij}^{\psi_{1j}\psi_{1j}} = \begin{bmatrix} 156 & 22l_{1j} & 54 & -13l_{1j} \\ 22l_{1j} & 4l_{1j}^2 & 13l_{1j} & -3l_{1j}^2 \\ 54 & 13l_{1j}^2 & 156 & -22l_{1j} \\ -13l_{1j} & -3l_{1j}^2 & -22l_{1j} & 4l_{1j}^2 \end{bmatrix}.$$

An alternative definition of the elementary mass matrix of the first link ($\mathbf{M}_{1j}$) of Eq. (4) can be written as:

$$\mathbf{M}_{1j} = \begin{bmatrix} m^{\phi_1\phi_1} & \mathbf{m}^{\phi_1\psi_{1j}} \\ \mathbf{m}^{\psi_{1j}\phi_1} & \mathbf{M}_{ij}^{\psi_{1j}\psi_{1j}} \end{bmatrix} \tag{5}$$

with $m^{\phi_1\phi_1} = m_{11}$, $\mathbf{m}^{\phi_1\psi_{1j}} = \begin{bmatrix} m_{12} & m_{13} & m_{14} & m_{15} \end{bmatrix}$, and $\mathbf{m}^{\psi_{1j}\phi_1} = \begin{bmatrix} m_{12} & m_{13} & m_{14} & m_{15} \end{bmatrix}^T$. Moreover:

$$\mathbf{K}_{1j} = \frac{EI}{l_{1j}^3} \begin{bmatrix} 0 & 0 & 0 & 0 & 0 \\ 0 & 12 & 6l_{1j} & -12 & 6l_{1j} \\ 0 & 6l_{1j} & 4l_{1j}^2 & -6l_{1j} & 2l_{1j}^2 \\ 0 & -12 & -6l_{1j} & 12 & -6l_{1j} \\ 0 & 6l_{1j} & 2l_{1j}^2 & -6l_{1j} & 4l_{1j}^2 \end{bmatrix} \tag{6}$$

Thus, the total kinematic and potential energy is defined as:

$$\begin{cases} T_1 = \frac{1}{2}\dot{\mathbf{q}}_1^T \mathbf{M}_1 \dot{\mathbf{q}}_1 \\ V_1 = \frac{1}{2}\mathbf{q}_1^T \mathbf{K}_1 \mathbf{q}_1 \end{cases} \tag{7}$$

Then, the global mass matrix and the global stiffness matrix ($\mathbf{M}_1$ and $\mathbf{K}_1$) are assembled based on the elementary matrices $\mathbf{M}_{1j}$, $\mathbf{M}_{m_{p1}}$, and $\mathbf{K}_{1j}$ for $j = 1, 2, \ldots, n_{1j}$ as described in [28, 29].

The Lagrangian is defined as $\mathscr{L}_1 = T_1 - V_1$. The dynamic equation of the manipulator is derived by applying the Lagrange principle of Eq. (8), thus:

$$\frac{d}{dt}\left[\frac{\partial \mathscr{L}_1}{\partial \dot{\mathbf{q}}_1}\right] - \frac{\partial \mathscr{L}_1}{\partial \mathbf{q}_1} = \mathbf{f}_1 \tag{8}$$

where $\mathbf{f}_1$ is the vector of the generalized non-conservative forces or moments. The development of the Lagrange equation (Eq. (8)) lead to the dynamic equation of the manipulator in the following form [30]:

$$\mathbf{M}_1(\mathbf{q}_1)\ddot{\mathbf{q}}_1 + \mathbf{h}_1(\mathbf{q}_1, \dot{\mathbf{q}}_1) + \mathbf{K}_1\mathbf{q}_1 = \mathbf{f}_1 \tag{9}$$

where $\mathbf{f}_1 = \begin{bmatrix} \tau_1 & \mathbf{0}_{1,2(n_{j1}-1)+2} \end{bmatrix}^T$ means that the input torque τ_1 is applied only on the joint ϕ_1. Moreover, $\mathbf{M}_1(\mathbf{q})$ is the total inertia matrix, $\mathbf{h}_1(\mathbf{q}_1, \dot{\mathbf{q}}_1)$ is the Coriolis/centripetal vector, and $\mathbf{K}_1$ is the total stiffness matrix.

The total mass matrix and the total stiffness matrix of Eq. (9) can be written in the following form:

$$\begin{cases} \mathbf{M}_1(\mathbf{q}_1) = \begin{bmatrix} m^{\phi_1\phi_1} & \mathbf{m}^{\phi_1\psi_1} \\ \mathbf{m}^{\psi_1\phi_1} & \mathbf{M}^{\psi_1\psi_1} \end{bmatrix} \\ \mathbf{K}_1 = \begin{bmatrix} 0 & \mathbf{0} \\ \mathbf{0} & \mathbf{K}^{\psi_1\psi_1} \end{bmatrix} \end{cases} \tag{10}$$

where $\mathbf{M}_{\psi_1\psi_1}$ is related to the transverse displacements or the elastic degrees of freedom of the links that correspond to $\boldsymbol{\psi}_1$; $\mathbf{m}_{\phi_1\psi_1}$ indicates the coupling between the joint ϕ_1 and these elastic degrees of freedom $\boldsymbol{\psi}_1$, and $\mathbf{m}_{\psi_1\phi_1} = \mathbf{m}_{\phi_1\psi_1}^T$; $m_{\phi_1\phi_1}$ takes into account the dynamics of the joint. Moreover, $\mathbf{K}_{\psi_1\psi_1}$ of the total stiffness matrix is the elementary stiffness matrix of the link; the total stiffness matrix does not have a coupling between the joint motion and the elastic degrees of freedom.

Moreover, the frequency domain response is also analyzed. The steady-state harmonic responses in the frequency domain can be used based on Eq. (9) by assuming harmonic inputs and outputs: $\mathbf{f}_1 = \mathbf{F}_1(\omega)e^{i\omega t}$ and $\mathbf{q}_1 = \mathbf{Q}_1(\omega)e^{i\omega t}$, with ω being the excitation frequency. It is worth mentioning that the total inertia matrix $\mathbf{M}_1(\mathbf{q}_1)$ depends only on joint variables ϕ_1 and the generalized velocities $\dot{\mathbf{q}}_{1j}$ are zero in the steady-state harmonic response. Thus, the Coriolis/centripetal $\mathbf{h}_1(\mathbf{q}_1, \dot{\mathbf{q}}_1)$ that depends on the generalized velocity is null. The following relationship between the amplitudes of the generalized forces and the amplitudes of the harmonic responses is obtained:

$$\mathbf{Q}_1(\omega) = \mathbf{H}(\omega)\mathbf{F}_1(\omega) \tag{11}$$

where $\mathbf{H}(\omega)$ is the receptance frequency response function matrix that is defined by:

$$\mathbf{H}(\omega) = \left[\mathbf{K}_1 - \omega^2\mathbf{M}_1(\mathbf{q}_1)\right]^{-1} \tag{12}$$

Stochastic Modeling

The uncertainty modeling is derived as an extension of the previously presented deterministic model. The uncertainties are considered on the dynamic parameters of the manipulator. Thus, the uncertainties are introduced first on the elementary matrices of mass $\mathbf{M}_{\psi_1\psi_1}$ and stiffness $\mathbf{K}_{\psi_1\psi_1}$ that affect the elastic degrees of freedom of the links ($\boldsymbol{\psi}_1$). The stochastic finite-element method proposed by [31] based on the spectral representation of the stochastic fields is used in the present contribution. Moreover, the lumped parameters, such as the tip mass, are modeled as random variables. Finally, the total mass and stiffness matrices with uncertainties are computed.

In the present contribution, the well-known Karhunen–Loéve (KL) expansion is used to model uncertainties of the mass and stiffness along with the links as stochastic fields. The Karhunen–Loéve (KL) decomposition is a spectral representation of the random fields that superposes the orthogonal random variables weighted by deterministic spatial functions [31]. A one-dimensional random field $H(x,\theta)$ is defined by its mean value, $E[H(x,\theta)]$, and its covariance function $C(x_1,x_2) = E\{[H(x_1,\theta) - E(x_1)][H(x_2,\theta) - E(x_2)]\}$, where x denotes the spatial dependence of the random field, $E[.]$ represents the expectation operator, and θ represents a random process. The one-dimensional homogeneous Gaussian random field $H(x,\theta)$ can be projected on an orthonormal truncated random function according to [31]:

$$H(x,\theta) = E(x) + \sum_{r=1}^{n_{KL}} \sqrt{\lambda_r} f_r(x)\xi_r(\theta) \tag{13}$$

where $f_r(x)$ and λ_r correspond to the deterministic eigenfunctions and the scalar eigenvalues of the covariance function $C(x_1,x_2)$, respectively. Moreover, it is worth defining that the eigenfunctions $f_r(x)$ and the random variables $\xi_r(\theta)$ are orthonormal.

The KL expansion is defined within the one-dimensional domain of the element where $\Omega_x = (x_1,x_2) \in x_{ij}$ to model the uncertain parameters of the element as random fields. Moreover, the analytical solution of the eigenproblem of the one-dimensional homogeneous Gaussian random field $H(x,\theta)$ was presented by [31] considering the exponential covariance function of Eq. (14).

$$C(x_1,x_2) = \exp\left(- \mid x_1 - x_2 \mid / l_{cor,x}\right) \tag{14}$$

where $(x_1,x_2) \in [0,l_j]$, l_j is the element length, and $l_{cor,y}$ is the correlation length that defines the decreasing behavior of the covariance with the distance between the points x_1 and x_2 in the x direction.

By considering the covariance function of Eq. (14), the solution of the eigenproblem lead to eigenfunctions $f_r(x)$ and the eigenvalues λ_r for $r = 1,2,\ldots,n_{KL}$. These eigenfunctions and eigenvalues depend on the r roots $\omega_r (r \geq 1)$ of two transcendental equations, as the following procedure summarizes:

- For the r odd, with $r \geq 1$, and $0 \leq x \leq l_j$:

$$\lambda_r = \frac{2l_{cor,x}}{l_{cor,x}^2\omega_r^2 + 1}, \quad f_r(x) = \alpha_r \cos(\omega_r x) \tag{15}$$

where $\alpha_r = 1/\sqrt{l_j/2 + \sin(\omega_r l_j)/2\omega_r}$ and the roots ω_r are obtained from the solution of the following transcendental equation:

$$1 + l_{cor,x}\omega_r \tan(\omega_r l_j) = 0$$

defined into the domain $\left[(r-1)\frac{\pi}{l_j}, \left(r - \frac{1}{2}\right)\frac{\pi}{l_j}\right]$.

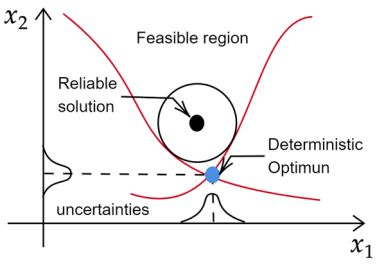

Fig. 2 Reliability-based optimization procedure, adapted from [26]

- For the r even, with $r \geq 1$, and $0 \leq x \leq l_j$:

$$\lambda_r = \frac{2l_{cor,x}}{l_{cor,x}^2\omega_r^2 + 1}, \quad f_r(x) = \alpha_r \sin(\omega_r x) \tag{16}$$

where $\alpha_r = 1/\sqrt{l_j/2 - \sin(\omega_r l_j)/2\omega_r}$ and the roots ω_r are obtained from the solution of the transcendental equation:

$$l_{cor,x}\,\omega_r + \tan(\omega_r l_j) = 0$$

defined into the domain $\left[\left(r - \frac{1}{2}\right)\frac{\pi}{l_j}, r\frac{\pi}{l_j}\right]$.

The KL expansion presented in Eqs. (13)–(16) has been used to model the random elementary random matrices of mass and stiffness; the uncertainties of the link are considered in the mass density ($\rho(\theta)$) and Young's modulus ($E(\theta)$):

$$\begin{cases} \mathbf{M}(\theta)^{\Psi_{1j}\Psi_{1j}} = \mathbf{M}_{\Psi_{1j}\Psi_{1j}} + \sum_{r=1}^{n_{KL}} \overline{\mathbf{M}}_r^{(s)} \rho(\theta) \\ \mathbf{K}(\theta)^{\Psi_{1j}\Psi_{1j}} = \mathbf{K}_{\Psi_{1j}\Psi_{1j}} + \sum_{r=1}^{n_{KL}} \overline{\mathbf{K}}_r^{(s)} E(\theta) \end{cases} \tag{17}$$

where $\mathbf{M}^{\Psi_{1j}\Psi_{1j}}$ and $\mathbf{K}^{\Psi_{1j}\Psi_{1j}}$ are the elementary mass matrix and stiffness matrix of Eqs. (5) and (6). Moreover, the random matrices $\overline{\mathbf{M}}_r^{(s)}(\theta)$ and $\overline{\mathbf{K}}_r^{(s)}(\theta)$ are calculated by using the following compact expression:

$$\begin{aligned} \overline{\mathbf{M}}_r^{(s)} &= \int_{x=0}^{l_j} \sqrt{\lambda_r} f_r(x)\mathbf{N}(x)^T\mathbf{N}(x)\mathrm{d}x \\ \overline{\mathbf{K}}_r^{(s)} &= \int_{x=0}^{l_j} \sqrt{\lambda_r} f_r(x)\mathbf{B}(x)^T\mathbf{B}(x)\mathrm{d}x \end{aligned} \tag{18}$$

with $\mathbf{N}(x) = \begin{bmatrix}\Phi_1 & \Phi_2 & \Phi_3 & \Phi_4\end{bmatrix}$ based on the shape functions of Eq. (2), and $\mathbf{B}(x) = \partial^2\mathbf{N}(x)/\partial x^2$.

Furthermore, the tip mass m_{p1} is typically affected by uncertainties. The uncertainty of $m_{p1}(\theta)$, $\rho(\theta)$ and $E(\theta)$ (of Eq. (17)) can be modeled as random variables. The uncertainties of these parameters can be defined as:

Table 1 Objective functions and constraints

Definition	Description
$f_1 = Pot = \max\left(\tau_1(t)\dot{\phi}_1(t)\right)$	Maximum power of joint actuator during the motion
$f_2 = m = \rho l_1 A + 2I_{m1}\pi/r_{m1}^2$	Mass of manipulator $r_{m1} = 0.01$m.
$f_3 = \sigma_{\omega_1} = \sqrt{\mathtt{var}(\omega_1(\theta))}$	Standard deviation of the first mode natural frequency[b]
$f_4 = R_f = P\left(\delta(\theta) - \delta^{(u)} \le 0\right)$	Reliability for the residual vibration (see Fig. 4c)[a]
$f_5 = y_t = \frac{f_t l_1^3}{3EI}$	Static tip deflection, for force of magnitude $f_t = 1$N.
$f_6 = \omega_1$, for $\lvert -\boldsymbol{\omega}^2\mathbf{M} + \mathbf{K} \rvert = 0$	First mode natural frequency
$h_1 = y_t - y^{(u)} = \frac{f_t l_1^3}{3EI} - y^{(u)}$	Constraint for static tip deflection[a]
$h_2 = \omega^{(l)} - \omega_1$, for $\lvert -\boldsymbol{\omega}^2\mathbf{M} + \mathbf{K} \rvert = 0$	Constraint for the first mode natural frequency[a]
$g_1 = \delta(\theta)$	Amplitude of residual vibration (see Fig. 7a).

[a] $\delta^{(u)}$ bounds to assess the reliability. $y^{(u)}$, and $\omega^{(l)}$ are defined as bounds for the constraints

[b] var(.) represents the variance of a random variable

$$\begin{aligned} m_{p1}(\theta) &= m_{p1} + m_{p1}\delta_{m_{p1}}\xi(\theta) \\ \rho(\theta) &= \rho + \rho\delta_{\rho}\xi(\theta) \\ E(\theta) &= E + E\delta_{E}\xi(\theta) \end{aligned} \tag{19}$$

where m_{p1}, E and ρ are the mean of these parameters, $\delta_{m_{p1}}$, δ_E and δ_ρ represents the dispersion level and $\xi(\theta)$ is the normal distributed random variable with θ being a random process that is governed by the normal distribution. The dynamic equation and the frequency response function are obtained:

$$\begin{cases} \mathbf{M}(\mathbf{q},\theta)\ddot{\mathbf{q}} + \mathbf{h}(\mathbf{q},\dot{\mathbf{q}},\theta) + \mathbf{K}(\theta)\mathbf{q} = \mathbf{f} \\ \mathbf{H}(\omega,\theta)\mathbf{F}(\omega) = \mathbf{Q}(\omega) \end{cases} \tag{20}$$

with:

$$\begin{cases} \mathbf{M}(\mathbf{q},\theta) &= \begin{bmatrix} m(\theta)^{\phi_1\phi_1} & \mathbf{m}(\theta)^{\phi_1\psi_1} \\ \mathbf{m}(\theta)^{\phi_1\psi_1} & \mathbf{M}(\theta)^{\psi_1\psi_1} \end{bmatrix} \\ \mathbf{K}(\theta) &= \begin{bmatrix} 0 & \mathbf{0} \\ \mathbf{0} & \mathbf{K}(\theta)^{\psi_1\psi_1} \end{bmatrix} \end{cases} \tag{21}$$

$\mathbf{h}_1(\mathbf{q},\dot{\mathbf{q}},\theta)$ is obtained from $\mathbf{M}_1(\mathbf{q},\theta)$.

Finally, the so-called Monte–Carlo Simulation (MCS) combined with the Latin Hypercube sampling [32] is the numerical method applied to obtain the dynamic response of the flexible manipulator with random parameters presented in Eq. (20).

Methodology for the Optimization Based on Reliability

The theoretical basis of reliability-based optimization (RBO) was introduced by Moses et al. [33]. The robust-based optimization (RBO) is presented in Eqs. (22)–(25) according to [26] where $f(.)$ represents the objective function, $\mathbf{x}_d$ is the vector of the determinist design variables, $\mathbf{x}_u(\theta)$ are the uncertain inputs modeled as random variables, and θ represents a stochastic process. This optimization problem is subject to the n_g reliability constraints of Eq. (23) where $P(.)$ denotes the joint probability of the solution being feasible for every j constraint by considering the uncertainties $\mathbf{x}_u(\theta)$, i.e., the reliability express the probability of obtaining a feasible solution under the uncertain inputs. $R \in [0,1]$ is the desired reliability for all jth constraints. The more reliable solution implies that R is close to one. $h_k(\mathbf{x}_d)$ of Eq. (24) denotes the deterministic inequality constraints, and Eq. (25) defines the constraints of the design variables.

$$\min_{\mathbf{x}_d} \quad f(\mathbf{x}_d, \mathbf{x}_u(\theta)) \tag{22}$$

$$\text{subject to} \quad P(g_j(\mathbf{x}_d, \mathbf{x}_u(\theta)) \le 0) \ge R, \quad j = 1, \ldots, n_g \tag{23}$$

$$h_k(\mathbf{x}_d) \le 0, \quad k = 1, \ldots, n_k \tag{24}$$

$$\mathbf{x}_d^{(l)} \le \mathbf{x}_d \le \mathbf{x}_d^{(u)} \tag{25}$$

Let us consider the optimization problem with two inequality constraints shown in Fig. 2. The deterministic optimal solution without uncertainty ($\mathbf{x}_u = 0$) is obtained by solving Eq. (22) and neglecting the reliability constraints of Eq. 23); one can observe that deterministic optimum is located at the intersection of the constraints. On the other hand, the reliability-based optimization problem considers the effect of uncertain inputs; these uncertain inputs produce variation around the optimal solution making this solution infeasible in many instances. Consequently, the reliable solution will be penalized by considering the reliability constraints of Eq. (23). A reliable solution will imply a small probability of obtaining an infeasible solution. The feasible solution with the desired reliability R will guarantee that the probability of obtaining an infeasible solution due to uncertainties is defined as $(1 - R)$.

The flexible manipulator's reliability-based optimization aims to optimize the performance under uncertainties. The geometric parameters can be considered design variables, and the uncertainties in the inertia and stiffness proprieties are considered. Several optimal criteria can be considered, e.g., maximizes the first mode natural frequency, minimizes the weight, or minimizes the elastic deflection at the tip. The effect of the uncertainties is quantified by a reliability index that expresses the probability of elastic deflection at the tip exceeding an imposed limit. The reliability should be maximized or constrained to the desired minimum bound.

Initially, the design variables are defined in the vector $\mathbf{x}_d = \begin{bmatrix} I_{m1} & h & b \end{bmatrix}$ with I_{m1} being the inertia of the cylindrical hub, and its mass is defined as $m_{m1} = 2I_{m1}\pi/r_{m1}^2$ where r_{m1} is the radius; h and b are the dimensions of the rectangle cross-section area of the link. The uncertain inputs parameters are defined in the vector $\mathbf{x}_u(\theta) = \begin{bmatrix} E(\theta) & \rho(\theta) & m_{p1}(\theta) \end{bmatrix}$. The link length ($l_1$) is defined according to the kinematic criterion.

Objective Functions and Constraints

The objective functions and constraints for the reliability-based optimization of the flexible manipulator are defined in Table 1. It is worth mentioning that these objective functions and constraints were defined based on the dynamic response of the flexible link manipulator with uncertain parameters using the stochastic finite element (see Sect. 2).

According to Table 1, f_i, for $i = 1, \ldots, 6$, defines the objective functions. The objective function $f_3 = \sigma_{\omega_1}$ is the standard deviation of the first mode natural frequency ω_1 that quantifies the effects of the uncertain parameters, i.e., it expresses how the dynamics vary by the uncertain parameters. $f_4 = R_f$ quantifies the reliability that consists of the probability of obtaining a vibration amplitude more minor than the limit $\delta^{(u)}$.

The constraints to $y^{(u)}$, h_1, the static deflection at the tip link (y_t) are subjected to the transversal tip force f_t, i.e., $\omega_1 > \omega^{(l)}$ $y_t \leq y^{(u)}$. Moreover, the constraint, h_2, imposes the minimum bound of $\omega^{(l)}$ for the first mode frequency ω_1, i.e., $\omega_1 > \omega^{(l)}$. Finally, the function g_1 denotes the residual vibration amplitude subject to uncertainties (see Fig. 7a), g_1 is used to assess the system reliability.

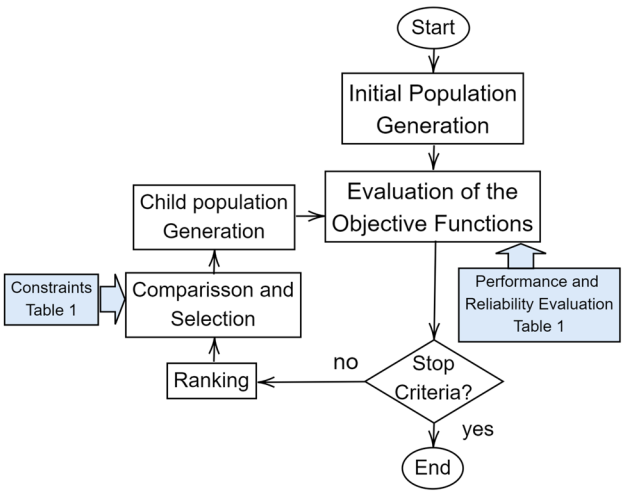

Fig. 3 Reliability optimization method

Assessment of the Reliability

The reliability-based optimization requires the efficient assessment of the system reliability defined in Eq. (23). For this particular application, the reliability quantifies the probability of amplitude of the residual vibration $\delta(\theta)$ (see Fig. 4d and Table 1) to be fewer than the desired limit defined as $\delta^{(u)}$. The mathematical definition of reliability expresses the probability of a given solution $\mathbf{x}_d$ to be safe under the jth constraint; the reliability can be written as $R = (1 - P_j)$:

$$P_j(\mathbf{x}_d, \mathbf{x}_u) = \int_{g_j(\mathbf{x}_d, \mathbf{x}_u)<0} f_{\mu_{\mathbf{x}_d}, \mu_{\mathbf{x}_d}}(\mathbf{x}_d, \mathbf{x}_u) \mathrm{d}\mathbf{x}_d \mathrm{d}\mathbf{x}_u \tag{26}$$

with P_j being the failure probability, and $f_{\mu_{\mathbf{x}_d}, \mu_{\mathbf{x}_d}}$ is the joint probability density function of $(\mathbf{x}_d, \mathbf{x}_u)$. There is not an analytical solution for the expression of Eq. (26) to obtain P_j.

Therefore, the First-Order Reliability Method (FORM) is used to estimate the failure probability P_j of Eq. (26). This method determines the point closest to the solution; this point is designated as the most probable point (MMP) of failure. First, the $\mathbf{x}$ coordinates systems are transformed into an independent standard normal coordinate system $\mathbf{u}$ using the Rosenblatt transformation [34].Then, the function $g_j(\mathbf{x}_d, \mathbf{x}_u) = 0$ or correspondingly $G_j(\mathbf{u}) = 0$ is approximated by a first-order Taylor at the MPP that corresponds to β_j. The reliability coefficient β is computed by solving the following optimization problem:

$$\begin{aligned} &\min_{\mathbf{u}} G_j(\mathbf{u}) \\ &\text{subject to:} \quad \beta_j = \| \mathbf{u}^T \mathbf{u} \| \end{aligned} \tag{27}$$

where $\| \cdot \|$ represents the magnitude of the vector. Finally, the probability of failure P_j is estimated according to the following expression: $P_j = \Phi[-\beta_j]$, where $\Phi[.]$ represents the standard normal cumulative distribution. The optimization problem to find the reliability coefficient β_j was solved by using the algorithm proposed by Rackwitz [35].

Fig. 4 Dynamic response

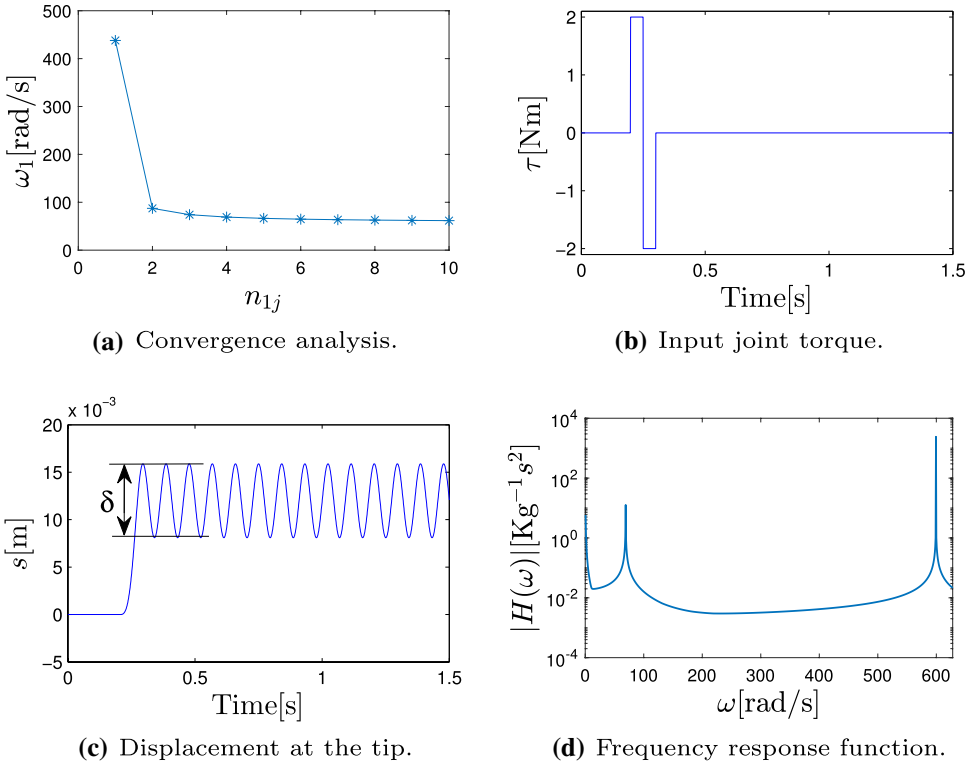

(a) Convergence analysis. **(b)** Input joint torque.

(c) Displacement at the tip. **(d)** Frequency response function.

Fig. 5 Eigenvalues and eigenfunction for the exponential covariance $C(x_1, x_2)$

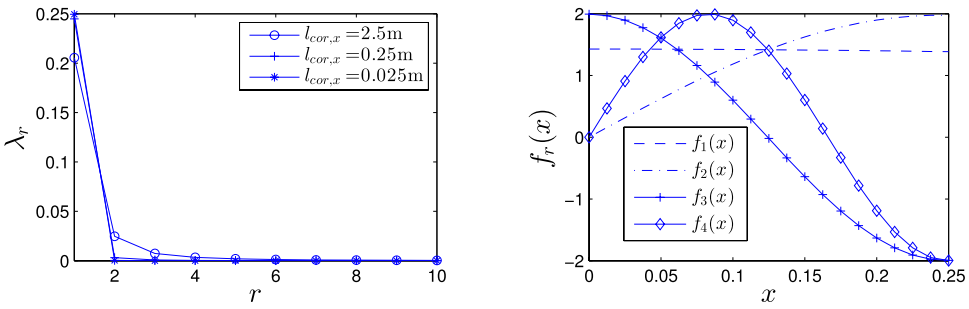

(a) Eigenvalues λ_r. **(b)** Eigenfunctions f_r.

Definition of the Reliability Optimization Problem

The reliability-based optimization of the flexible manipulator consists of maximizing the objective functions subject to reliability constraints. Consequently, three types of reliability-based optimizations were proposed: (I) single-objective RBO (see Eq. (28a)): maximizes one single objective function by imposing reliability constraints and operational constraints; (II) multi-objective RBO to maximize reliability (see Eq. (28b)): optimizes simultaneously one objective function and maximizes the reliability, and (III) multi-objective RBO with reliability constraints (see Eq. (28c)): optimization of two objectives simultaneously

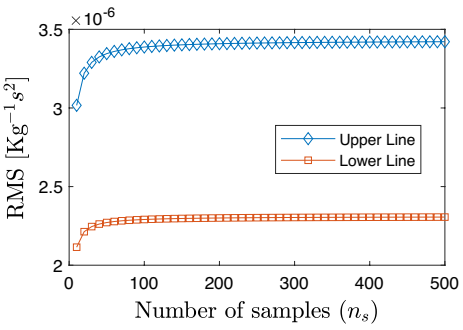

Fig. 6 Convergence of the maximum error for the numbers of samples (n_s) used in the MCS

Table 2 Reliability outputs using MCS and FORM methods

$\mathbf{x}_d = [I_{m1} \;\; h \;\; b]$	R_f (MCS)	R_f(FORM)	n_f (MCS)	n_f (FORM)
$[2\times10^{-5} \;\; 0.0025 \;\; 0.0290]$	0.7113	0.7268	15000	73
$[2\times10^{-5} \;\; 0.0020 \;\; 0.0290]$	0.3121	0.3212	15000	74
$[2\times10^{-5} \;\; 0.0010 \;\; 0.0290]$	0.0181	0.0178	15000	57
$[5\times10^{-5} \;\; 0.0025 \;\; 0.0290]$	0.6913	0.6870	15000	55
$[5\times10^{-5} \;\; 0.0020 \;\; 0.0290]$	0.3120	0.3212	15000	75
$[5\times10^{-5} \;\; 0.0010 \;\; 0.0290]$	0.0219	0.0178	15000	58
$[5\times10^{-5} \;\; 0.0025 \;\; 0.0250]$	0.0928	0.0934	15000	127
$[5\times10^{-5} \;\; 0.0010 \;\; 0.0250]$	0.0008	0.0000	15000	72
$[5\times10^{-6} \;\; 0.0025 \;\; 0.0270]$	0.2965	0.2978	15000	95
$[5\times10^{-6} \;\; 0.0010 \;\; 0.0270]$	0.0010	0.0000	15000	79

with reliability constraints. The presented RBO demands the solution of multi-objective optimization problems; for this end, evolutionary algorithms have been integrated into RBO [26]. The single-objective optimization of Eq. (28a) serves as a baseline to compare the reliability optimization of Eqs. (28b) and (28c); this optimization is solved using the genetic algorithm [36].

Type I:

$$\begin{aligned} &\min_{\mathbf{x}_d} f_i(\mathbf{x}_d, \boldsymbol{\mu}_u) \\ &\text{subject to } P(g_1(\mathbf{x}_d, \mathbf{x}_u(\theta)) - \delta^u \le 0) \ge R \\ &\qquad h_k(\mathbf{x}_d) \le 0, \quad k = 1,2 \\ &\qquad \mathbf{x}_d^{(l)} \le \mathbf{x}_d \le \mathbf{x}_d^{(u)} \end{aligned} \tag{28a}$$

Type II:

$$\begin{aligned} &\min_{\mathbf{x}_d} f_i(\mathbf{x}_d, \boldsymbol{\mu}_u) \qquad \max_{\mathbf{x}_d} f_4(\mathbf{x}_d, \mathbf{x}_u(\theta)) \\ &\text{subject to } h_k(\mathbf{x}_d) \le 0, \quad k = 1,2 \\ &\qquad \mathbf{x}_d^{(l)} \le \mathbf{x}_d \le \mathbf{x}_d^{(u)} \end{aligned} \tag{28b}$$

Type III:

$$\begin{aligned} &\min_{\mathbf{x}_d} f_i(\mathbf{x}_d, \boldsymbol{\mu}_u) \qquad \min_{\mathbf{x}_d} f_j(\mathbf{x}_d, \boldsymbol{\mu}_u) \quad \text{with} \quad i \ne j \\ &\text{subject to } P(g_j(\mathbf{x}_d, \mathbf{x}_u(\theta)) - \delta_{max} \le 0) \ge R, \quad j = 1, \ldots, n_g \\ &\qquad \mathbf{x}_d^{(l)} \le \mathbf{x}_d \le \mathbf{x}_d^{(u)} \end{aligned} \tag{28c}$$

The multi-objective optimizations derived from the reliability optimization of Eqs. (28b) and (28c) are solved using the NSGA-II multi-objective genetic algorithm [37], because this optimization technique has been successfully applied to optimize robotic systems [7, 38]. The reliability optimization methodology works in the following way (see Fig. 3): (i) an initial population that is a set of solutions is generated randomly within the design space. (ii) evaluates the objective functions based on the performance criteria and reliability (see Table 1); (iii) a child population is generated by ranking, selecting and applying the genetic operators (crossover and mutation); (iv) evaluates the stop criteria to determine if the optimization process converges; if the stop criteria are not met, the process is repeated since step (ii).

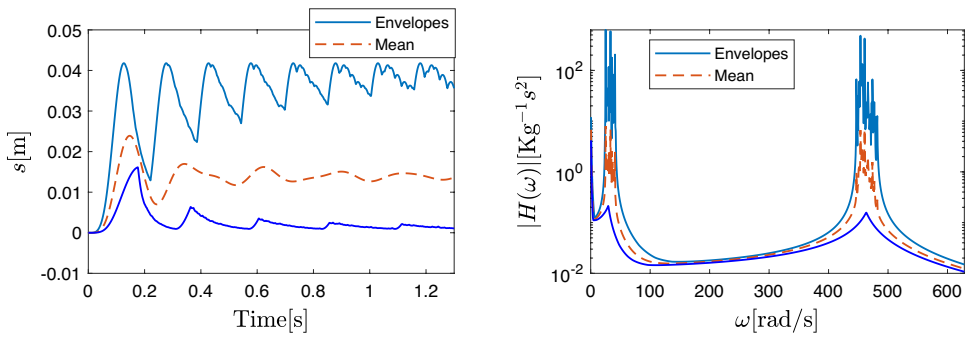

Fig. 7 Dynamic response with uncertainties

(a) Displacement at the tip.

(b) Frequency response function.

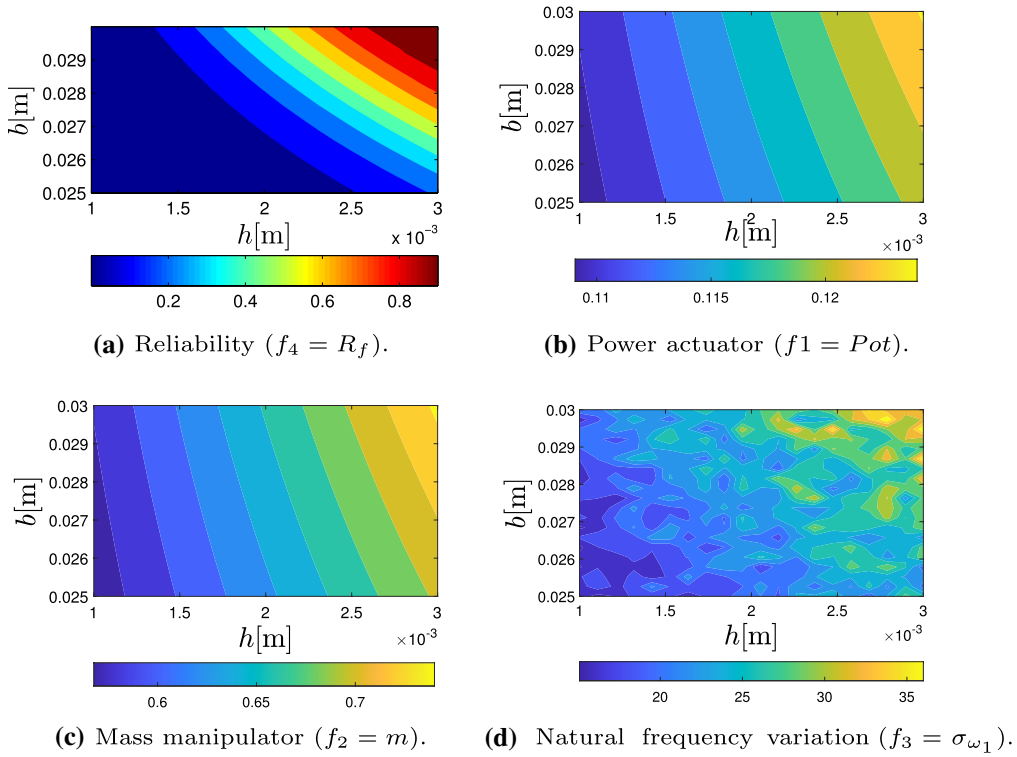

(a) Reliability ($f_4 = R_f$). **(b)** Power actuator ($f1 = Pot$).

(c) Mass manipulator ($f_2 = m$). **(d)** Natural frequency variation ($f_3 = \sigma_{\omega_1}$).

Fig. 8 Reliability as a function of design variables h and b

Table 3 Reliability-based optimization (RBO) of the flexible manipulator

RBO Type		Optimization Problem	Description	Constraints
I	(a)	$\min Pot$	Minimization of actuator power	$R_f \geq R^{(l)}\, y_t - y^{(u)} \leq 0\, \omega^{(l)} - \omega_1 \leq 0$
	(b)	$\min m$	Minimization of manipulator mass	
	(c)	$\min \sigma_{\omega_1}$	Minimization of first mode frequency standard deviation	
II	(d)	$\min Pot \max R_f$	Minimization of actuator power and maximization of reliability	$y_t - y^{(u)} \leq 0\, \omega^{(l)} - \omega_1 \leq 0$
	(e)	$\min m \max R_f$	Minimization of mass and maximization of reliability	
	(f)	$\min \sigma_{\omega_1} \max R_f$	Minimization of first mode frequency variation and maximization of reliability	
III	(g)	$\min Pot \min y_t$	Minimization of actuator power and minimization of link deflection	$R_f \geq R^{(l)}$
	(h)	$\min Pot \max \omega_1$	Minimization of mass and maximization of first mode frequency	

$y^{(u)} = 0.002$ m, and $\omega^{(l)} = 70$ rad/s are the as bounds for the constraints. $\delta^{(u)} = 0.001$ m is the maximum limit to assess the reliability of Eqs. (28a) and (28c).

R_f is defined according to each optimization

Numerical Results

The results of the flexible manipulator illustrate the dynamics of Sect. 2.1, the modeling with uncertainties of Sect. 2.2, and the reliability optimization methodology of Sect. 3.

Flexible Manipulator Dynamics

The parameters considered for the one link-flexible manipulator are presented in Table 5. The link length is defined as l_i =1m. It is worth mentioning that the cross-section area of the link is defined as a rectangle with dimensions

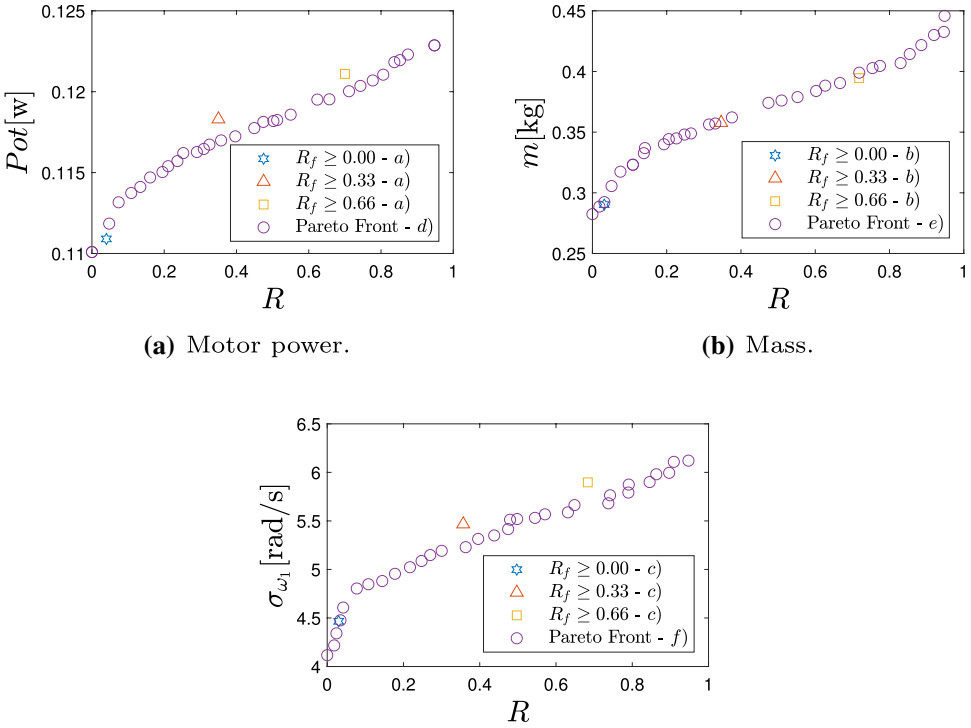

(a) Motor power. **(b)** Mass.

(c) First mode natural frequency variation.

Fig. 9 Pareto Fronts for type I and type II optimization

$h = 0.003$m by $b = 0.02$m; the area is defined as $A = bh$, and the moment of inertia $I = bh(b^2 + h^2)/12$.

Initially, the number of elements (n_{1j}) necessary to compute the dynamic response using the finite-element method is verified by evaluating the convergence of the first mode natural frequency (ω_1). Figure 4a shows the first mode natural frequency (ω_1) as a function of the number of elements (n_{1j}). The convergence is obtained for $n_{1j} \geq 4$ since ω_1 does not exhibit an expressive variation.

The dynamic response of the manipulator is evaluated without considering the uncertainties. The displacement of the tip (see Fig. 4c) is obtained by integrating the total dynamic equation of Eq. (9); the manipulator starts its motion at the rest, the initial joint position is $\phi_1 = 0$, and the torque τ_1 is applied (see Fig. 4b). The motion of the tip produced by τ_1 exhibits a vibration that persists. This residual vibration of the tip arises from the link flexibility, and its amplitude is characterized as δ (see Fig. 4c). Moreover, the amplitude of the frequency response function (FRF) is presented in Fig. 4d by following the expression presented in Eq. (12). The first and second natural frequency corresponds to 69.06 and 599.41 rad/s, respectively.

Flexible Manipulator Dynamics with Uncertainties

As an example to illustrate the KL expansion, Fig. 5 shows the eigenfunctions $f_r(x)$ and λ_r eigenvalues (see Eqs. (15)

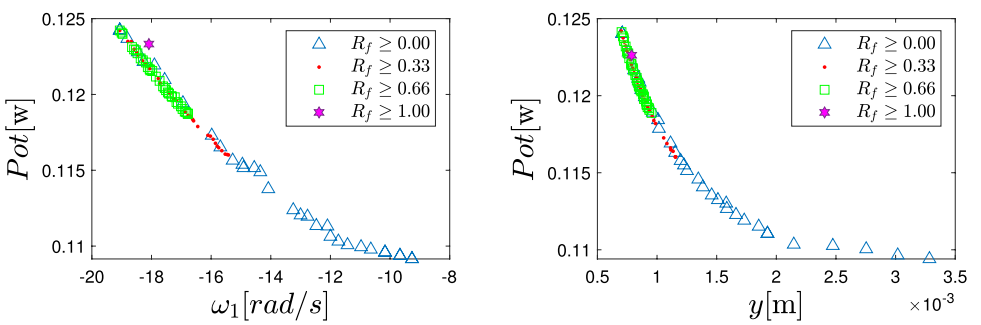

(a) Motor power and first mode frequency. **(b)** Motor power and static tip deflection.

Fig. 10 Pareto Fronts for the Type III optimization

Table 4 Results of the RBO of the flexible manipulator

RBO type		Decision space $\mathbf{x}_d = [I_{m1}\ \ h\ \ b]$	Criterion space f_i	Reliability constraints bounds
I	(a)	$[5.4130 \times 10^{-6}\ \ 0.0011\ \ 0.0300]$	$Pot = 0.1107$ w	$R^{(l)} = 0.00$
	(a)	$[2.8435 \times 10^{-5}\ \ 0.0023\ \ 0.0280]$	$Pot = 0.1180$ w	$R^{(l)} = 0.33$
	(a)	$[2.2932 \times 10^{-5}\ \ 0.0027\ \ 0.0284]$	$Pot = 0.1209$ w	$R^{(l)} = 0.66$
	(b)	$[5.1172 \times 10^{-6}\ \ 0.0011\ \ 0.0295]$	$m = 0.2903$ kg	$R^{(l)} = 0.00$
	(b)	$[5.5506 \times 10^{-6}\ \ 0.0018\ \ 0.0301]$	$m = 0.3578$ kg	$R^{(l)} = 0.33$
	(b)	$[5.4070 \times 10^{-6}\ \ 0.0023\ \ 0.0299]$	$m = 0.3945$ kg	$R^{(l)} = 0.66$
	(c)	$[7.9813 \times 10^{-6}\ \ 0.0017\ \ 0.0259]$	$\sigma_{\omega_1} = 4.4654$ rad/s	$R^{(l)} = 0.00$
	(c)	$[4.2563 \times 10^{-5}\ \ 0.0030\ \ 0.0259]$	$\sigma_{\omega_1} = 5.4665$ rad/s	$R^{(l)} = 0.33$
	(c)	$[3.6548 \times 10^{-5}\ \ 0.0028\ \ 0.0280]$	$\sigma_{\omega_1} = 5.8974$ rad/s	$R^{(l)} = 0.66$
II	(d)	–	Pareto front (Fig 9a)	–
	(e)	–	Pareto front (Fig 9c)	–
	(f)	–	Pareto front (Fig 9b)	–
III				$R^{(l)} \geq \begin{cases} 0.00 \\ 0.33 \\ 0.66 \\ 1.00 \end{cases}$
	(g)	–	Pareto front (Fig 10a)	
	(h)	–	Pareto front (Fig 10b)	

and (16)) of the exponential covariance function in Eq. (14). Initially, the first ten eigenvalues were computed for $\Omega_x = (0, 0.25)$ m, and three different correlation lengths: $l_{cor,x}$ =2.5, 0.25 and 0.025 m. It observed that the KL expansion could approximate the random field by considering the four first eigenvalues (see Fig. 5a) since the eigenvalues are negligible for $n_{KL} > 4$. Moreover, the first four eigenfunctions (for n_{KL} =4) are presented in Fig. 5b by considering $\Omega_x = 0, 0.25$ m and $l_{cor,x}$ =0.25 m.

The number of samples (n_s) to obtain an accurate output in the Monte–Carlo simulation is verified by evaluating the convergence of the response variability of the stochastic response $\hat{H}(\omega, \theta)$. The mean square convergence (*RMS*) of the FRF amplitude is assessed as a function of the number of the realization of θ, i.e., samples (n_s). The following expression for the *RMS* is considered:

$$RMS = \sqrt{\frac{1}{n_s} \sum_{n=1}^{n_s} | \hat{H}(\omega, \theta) - H(\omega) |^2} \tag{29}$$

with $H(\omega)$ being the amplitude of the FRF. The lower and upper limits of the envelopes of the random amplitude of the *RMS* are presented in Fig. 6 based on Eq. (29). The convergence is obtained for $n_s \geq 80$. Moreover, for this simulation the correlation length is equal to the element length, thus ($l_{cor,x} = l_{1j}$). Therefore, the eigenvalues for $\lambda_r \geq 5$ are negligible based on the results presented in Fig. 5a by considering these definitions.

Therefore, for the following simulations that consider the stochastic finite-element: n_{KL} =4, $l_{cor,x}$ =0.25m and n_s =100.

The uncertainties were introduced in the mass density link $\rho(\theta)$ and Young's modulus $E(\theta)$ and the mass at the tip of the link $m_{p1}(\theta)$. According to the expression that defined the random variable of Eq. (19) the mean of the parameters corresponds to the afore defined values; the dispersion level of 5% for δ_ρ and δ_E, and 20% for $\delta_{m_{p1}}$.

The dynamic response was also computed considering the uncertainties in the mass at the tip m_{p1}, Young's modulus E, and the links' mass density ρ. The envelopes of Fig. 7 represent the maximum and the minimum limits of the response variability produced by the uncertainties. The envelopes of displacement of the tip subjected to the same initial conditions and torque inputs are presented in Fig. 7a; one can observe that small uncertainty produces a remarkable variation in the residual vibration amplitude δ. Furthermore, the frequency response function subjected to uncertainties was also analyzed (see Fig. 7b), and one can observe that the uncertainties produce significant variation in the vibration modes.

Optimal Design Results

The parameters of the flexible manipulator used for the numerical simulations are presented in Table 5. The reliability R is assessed within the bounds of the cross-section

area dimensions b and h (see the design variables definition of Table 6).

The accuracy of the FORM to estimate the reliability for residual vibrations (R_f of Table 1) is evaluated considering the MCS (Monte–Carlo Simulation) as the reference according to [39]. Table 2 presents the outcomes of the reliability for residual vibrations, R_f, in Table 2. One can observe that R_f obtained using FORM and MCS are similar in most cases since FORM copes properly with the nonlinearity of the dynamic model of the flexible manipulator. Moreover, n_f represents the number that every method demands the computation of the dynamic model to estimate the reliability (R_f). One can observe that FORM requires less computation cost than MCS, as presented in Table 2.

In Fig. 8a one can observe that the reliability augments with the increasing cross-section area of the link, i.e., the more cross-section area decreases the amplitude of the residual vibration at the tip, and thus reliability.

In addition, the objective functions (f_1, f_2, and f_3) are also assessed as a function of the design variables of Table 1. The optimization demands the maximization of the reliability (f_4), and simultaneously, it minimizes the power of the joint actuators (f_1), the mass (f_2), and the natural frequency variation (f_3). One can observe that the objective functions exhibit an opposite behavior to the reliability f_4, i.e., the increase in reliability implies an increase of the power of the joint actuators (see Fig. 8b), the mass (see Fig. 8c) and the variability of the first mode natural frequency (see Fig. 8d).

Table 3 presents the application of the reliability-based optimization (RBO) to the flexible manipulator described based on Eqs. (28a)–(28c). The type I RBO aims at minimizing a single objective (a) actuator power, (b) manipulator mass, and (c) variation on the first mode natural frequency) subject to the following constraints: minimum desired reliability $R^{(l)}$, maximum static tip deflection $y^{(u)}$ and minimum first mode natural frequency $\omega^{(l)}$. The type II RBO maximizes the reliability and minimizes the (d) actuator power, (e) manipulator mass, and (f) variation on the first mode natural frequency subject to the following constraints: maximum static tip deflection $y^{(u)}$ and minimum first mode natural frequency $\omega^{(l)}$. Finally, two objective functions are optimized simultaneously subject to the minimum desired reliability $R^{(l)}$: (g) minimizes the actuator power and minimizes the static tip deflection, and (h) minimizes the actuator power and maximizes the first mode natural frequency.

The RBO optimization problems of Table 3 were solved by using evolutionary algorithms according to the approach presented by Deb et al. [26]. Specifically, the genetic algorithms were used for optimizations (a), (b) and (c) (see Table 3), and multi-objective genetic algorithm NSGA-II [37] for optimizations (d)–(h) (see Table 3). The parameters of the flexible manipulator and the constraints are defined in Tables 5 and 6, respectively. The following parameters were selected for the NSGA-II: population size has 45, 100 generations, tournament selection strategy, crossover rate is 0.8, the Pareto fraction is 0.35, and the migration factor is 0.1.

The solutions of single-objective optimization (Type I) and multi-objective (Type II) are presented in Fig.9. As presented in Fig. 8 the reliability R_f and the actuator power Pot, manipulator mass m are opposite objectives. Thereby, the multi-objective optimization Type II solution derives the Pareto Front, which expresses a set of optimal solutions for these contradictory objectives. The designer can select a single solution to minimize the objective function with the desired reliability; e.g., the design variables to minimize the actuator power for the desired reliability can be selected. Moreover, one can observe that the solution of Type I optimization attains results closed to the Pareto front for several minimum desired reliabilities: $R^{(l)} = 0.00$, $R^{(l)} = 0.33$ and $R^{(l)} = 0.66$. Type I optimization leads to a single solution instead of type II optimization establishes a set of solutions that optimally balances the opposite objective functions. For type II, one can observe the actuator power and reliability (see Fig. 9a), mass, and reliability (see Fig. 9b), and variation of the first mode frequency and reliability (see Fig. 9c). These optimizations allowed us to obtain the dimensions of the cross-section area and hub inertia to minimize the effects of the link flexibility and increase the reliability simultaneously.

The set of the optimal solutions corresponding to Type III optimization are presented in Fig. 10 for the following minimum desired reliabilities: $R^{(l)} = 0.00$, $R^{(l)} = 0.33$ and $R^{(l)} = 0.66$. These optimizations minimize the power of the joint actuator and maximize the first mode frequency (see Fig. 10a), and minimizes the static deflection of the tip (see Fig. 10a) subject to the desired reliability (R_f). The optimal solutions are superposed over the Pareto front. Increasing the minimum reliability (R_f) decreases the number of elements of the optimal solution set. Thus results are obtained because the reliability definition for this application imposes constraints on the dynamic behavior of the manipulator, i.e., the reliability depends on the amplitude of residual vibration subject to uncertainties. This optimization approach can also be applied to the other objective functions considered in Table 1, such as the mass of the manipulator or the variation of the first mode natural frequency.

The definition of the design variables $\mathbf{x}_d$ obtained by applying the reliability-based optimization is presented in Table 4. Moreover, the definition of the objective function for the corresponding reliability constraint is also presented. The design variables define the dimensions of the cross-section area and the inertia of the hub. by selecting these parameters, the dynamic response of the manipulator can be optimized, and the reliability of vibration amplitude at the tip can also be constrained.

Conclusion

This contribution presents an optimal design procedure for a flexible-link manipulator subject to uncertainty parameters to optimize dynamic performance and reliability. The proposed approach permits optimizing the main characteristics of the flexible link manipulator, such as the actuator's power, mass, and tip deflection based on the elastic dynamic model. The objective functions consider the dynamic response of the manipulator in the frequency domain and the time domain.

The proposed modeling of the flexible-link manipulator permitted includes the uncertainties on the links' parameters mass, stiffness, and damping parameters by applying the stochastic finite-element method. Moreover, the dynamic response subjected to uncertainties is obtained using the Monte–Carlo simulation. The reliability was efficiently computed based on the uncertain model of the manipulator and the first-order reliability method. The proposed modeling approach to the uncertainties of the links can also be extended to manipulators with multiple degrees of freedom.

The proposed optimization aims to optimize key operational characteristics of flexible manipulators, such as minimizing the elastic deflections, the power of actuators, and the mass of the manipulator subject to reliability constraints. Therefore, these operational characteristics are optimized subject to uncertainties by including reliability as a measure of robustness, i.e., the manipulator is less sensitive to uncertainties by maximizing the reliability criterion. Unlike the single-objective optimization procedure, the multi-objective genetic algorithm to solve the optimization problem lets solve two opposite objectives subject to constraints. The set of the optimal solutions and its corresponding definitions of the design variables are obtained to optimize the dynamic performance. Moreover, the optimization procedure can also include operational constraints based on the elastodynamic performance.

Consequently, the novel contributions of the proposed method can be summarized in two main points based on the results. First, the stochastic modeling of flexible-link manipulators allows including the uncertain structural parameters and computing the dynamical response. Finally, the reliability optimization approach applied to the one-link flexible manipulator with uncertain structural parameters permitted to obtain the inertial and geometric parameters to optimize the elastodynamic performance subjected to uncertainties.

Future works will encompass the optimization of multi-degrees of freedom flexible-link manipulators considering control system criteria.

Appendix A Parameters of Flexible-Link Manipulator

See Tables 5, 6.

Table 5 Physical and geometric parameters of flexible-link manipulator

Properties	Nomenclature	Unit	Values
Young's modulus	E	N/m^2	7×10^{10}
Mass density	ρ	kg/m^3	2700
Dimension of rectangular cross-section	h	m	0.02
Dimension of rectangular cross-section	b	m	0.003
Cross-section area	A	m^2	bh
Cross-section inertia	I	m^4	$bh\frac{b^2+h^2}{12}$
Hub inertia	I_{m1}	kg m^2	0.1
Radius of the cylindrical hub	r_{m1}	m	0.01
Link length	l_1	m	1
Number of elements	n_{1j}	-	4
Tip mass	m_{p1}	kg	0.1

Table 6 Definition bounds of optimization constraits

Properties	Nomenclature	Unit	Values
Maximum residual vibration amplitude to assess the reliability	$\delta^{(u)}$	m	0.001
Maximum static tip deflection	$y^{(u)}$	m	0.002
Minimum fist mode natural frequency	$\omega^{(l)}$	rad/s	70
Minimum bound of the design variables	$\mathbf{x}_d^{(l)}$	$[kg\,m^2\ m\ m]$	$[5\times10^{-6}\ 0.001\ 0.025]$
Maximum bound of the design variables	$\mathbf{x}_d^{(u)}$	$[kg\,m^2\ m\ m]$	$[5\times10^{-5}\ 0.003\ 0.030]$

Acknowledgements The authors are thankful for the financial support provided by CNPq (Process 427204/2018-6), and CAPES.

Declarations

Conflict of interest This study was funded by CNPq (427204/2018-6) and, CAPES. The authors declare that they have no conflict of interest.

References

1. Omisore OM, Han S, Xiong J, Li H, Li Z, Wang L (2020) A review on flexible robotic systems for minimally invasive surgery. IEEE Trans Syst Man Cybern Syst
2. She Y, Song S, Su H-J, Wang J (2021) A parametric study of compliant link design for safe physical human–robot interaction. Robotica 39(10):1739–1759
3. Thomsen DK, Søe-Knudsen R, Balling O, Zhang X (2021) Vibration control of industrial robot arms by multi-mode time-varying input shaping. Mech Mach Theory 155:104072
4. Sayahkarajy M, Mohamed Z, Mohd Faudzi AA (2016) Review of modelling and control of flexible-link manipulators. Proc Inst Mech Eng I J Syst Control Eng 230(8):861–873
5. Benosman M, Le Vey G (2004) Control of flexible manipulators: a survey. Robotica 22(5):533–545
6. Dixit US, Kumar R, Dwivedy SK (2005) Shape optimization of flexible robotic manipulators. J Mech Des 128(3):559–565. https://doi.org/10.1115/1.2181606
7. Lara-Molina FA, Dumur D, Takano KA (2018) Multi-objective optimal design of flexible-joint parallel robot. Eng Comput
8. Beyer H-G, Sendhoff B (2007) Robust optimization—a comprehensive survey. Comput Methods Appl Mech Eng 196(33–34):3190–3218
9. Sun T, Lian B, Song Y, Feng L (2019) Elastodynamic optimization of a 5-dof parallel kinematic machine considering parameter uncertainty. IEEE/ASME Trans Mechatron 24(1):315–325
10. Lara-Molina FA, Dumur D (2021) Robust multi-objective optimization of parallel manipulators. Meccanica 56(11):2843–2860
11. Valdebenito MA, Schuëller GI (2010) A survey on approaches for reliability-based optimization. Struct Multidiscip Optim 42(5):645–663
12. Bowling AP, Renaud JE, Newkirk JT, Patel NM, Agarwal H (2006) Reliability-based design optimization of robotic system dynamic performance. J Mech Des 129(4):449–454. https://doi.org/10.1115/1.2437804
13. Fei C, Liu H, Patricia Liem R, Choy Y, Han L (2022) Hierarchical model updating strategy of complex assembled structures with uncorrelated dynamic modes. Chin J Aeronaut 35(3):281–296. https://doi.org/10.1016/j.cja.2021.03.023
14. Fei C-W, Li H, Lu C, Han L, Keshtegar B, Taylan O (2022) Vectorial surrogate modeling method for multi-objective reliability design. Appl Math Model 109:1–20. https://doi.org/10.1016/j.apm.2022.03.033
15. Fei C-W, Li H, Liu H-T, Lu C, Keshtegar B, An L-Q (2020) Multilevel nested reliability-based design optimization with hybrid intelligent regression for operating assembly relationship. Aerosp Sci Technol 103:105906. https://doi.org/10.1016/j.ast.2020.105906
16. Li H, Bu S, Wen J-R, Fei C-W (2022) Synthetical modal parameters identification method of damped oscillation signals in power system. Appl Sci 12(9)
17. Fei C-W, Li H, Liu H-T, Lu C, An L-Q, Han L, Zhao Y-J (2020) Enhanced network learning model with intelligent operator for the motion reliability evaluation of flexible mechanism. Aerosp Sci Technol 107:106342. https://doi.org/10.1016/j.ast.2020.106342
18. Lara-Molina FA, Dumur D (2021) A fuzzy approach for the kinematic reliability assessment of robotic manipulators. Robotica 39(12):2095–2109
19. Zhang C-Y, Song L-K, Fei C-W, Hao G-P, Liu L-J (2016) Reliability-based design optimization for flexible mechanism with particle swarm optimization and advanced extremum response surface method. J Central South Univ 23(8):2001–2007
20. Zhao Y, Lu C, Fei C, An L, Hu Y, Huang B, Yuan L (2020) Transient reliability evaluation approach of flexible mechanism with ga-extremum neural network. Math Problems Eng 2020
21. Bai B, Zhou C, Ye N, Liu X, Li W (2022) Reliability optimization of two-link flexible manipulator. Appl Math Model 101:76–95
22. Ling M, Cao J, Li Q, Zhuang J (2018) Design, pseudostatic model, and pvdf-based motion sensing of a piezo-actuated xyz flexure manipulator. IEEE/ASME Trans Mechatron 23(6):2837–2848
23. Liao B, Gao X, Lou Y (2021) An integrated structure and control design of a coaxis planar parallel manipulator for pick-and-place applications based on elastic potential energy. Int J Adv Rob Syst 18(5):17298814211049124
24. Lismonde A, Sonneville V, Brüls O (2019) A geometric optimization method for the trajectory planning of flexible manipulators. Multibody Syst Dyn 47(4):347–362
25. Korayem MH, Nikoobin A, Azimirad V (2009) Trajectory optimization of flexible link manipulators in point-to-point motion. Robotica 27(6):825–840
26. Deb K, Gupta S, Daum D, Branke J, Mall AK, Padmanabhan D (2009) Reliability-based optimization using evolutionary algorithms. IEEE Trans Evol Comput 13(5):1054–1074
27. Usoro PB, Nadira R, Mahil SS (1986) A finite element/lagrange approach to modeling lightweight flexible manipulators. J Dyn Syst Meas Contr 108(3):198–205
28. Inman DJ, Singh RC (1994) Engineering vibration, vol 3. Prentice Hall Englewood Cliffs, NJ, Upper Saddle River, New Jersey
29. Meirovitch L (1980) Computational methods in structural dynamics, vol 5. Springer, Berlin
30. Lewis FL, Dawson DM, Abdallah CT (2003) Robot manipulator control: theory and practice. CRC Press, New York, NY
31. Ghanem RG, Spanos PD (2003) Stochastic finite elements: a spectral approach. Courier Corporation, Mineola, NY
32. Florian A (1992) An efficient sampling scheme: updated latin hypercube sampling. Probab Eng Mech 7(2):123–130
33. Moses F, Kinser DE (1967) Optimum structural design with failure probability constraints. AIAA J 5(6):1152–1158
34. Rosenblatt M (1952) Remarks on a multivariate transformation. Ann Math Stat 23(3):470–472
35. Rackwitz R (1976) Practical probabilistic approach to design. Bulletin, 112. Comite European du Beton
36. Holland JH (1973) Genetic algorithms and the optimal allocation of trials. SIAM J Comput 2(2):88–105
37. Deb K, Pratap A, Agarwal S, Meyarivan T (2002) A fast and elitist multiobjective genetic algorithm: NSGA-II. IEEE Trans Evol Comput 6(2):182–197

38. Yusoff Y, Ngadiman MS, Zain AM (2011) Overview of nsga-ii for optimizing machining process parameters. Proc Eng 15:3978–3983
39. Chen Z, Wu Z, Li X, Chen G, Chen G, Gao L, Qiu H (2019) An accuracy analysis method for first-order reliability method. Proc Inst Mech Eng C J Mech Eng Sci 233(12):4319–4327